Bismuth Islands for Low-temperature Sodium-beta Alumina Batteries

Dana Jin, Sangjin Choi, Woosun Jang, Aloysius Soon, Jeongmin Kim, Hongjae Moon, Wooyoung Lee, Younki Lee, Sori Son, Yoon Cheol Park, Hee Jung Chang, Guosheng Li, Keeyoung Jung, and Wooyoung Shim

Just Accepted

1
2
3
4
5
6
7
8
9
10
11
12
13
14
15
16
17
18
19
20
21
22
23
24
25
26
27
28
29
30
31
32
33
34
35
36
37
38
39
40
41
42
43
44
45
46
47
48
49
50
51
52
53
54
55
56
57
58
59
60

Bismuth Islands for Low-temperature Sodium-beta Alumina Batteries

Dana Jin[†], Sangjin Choi[†], Woosun Jang[†], Aloysius Soon[†], Jeongmin Kim[†], Hongjae Moon[†], Wooyoung Lee[†], Younki Lee[‡], Sori Son[§], Yoon-Cheol Park[§], HeeJung Chang[∥], Guosheng Li[∥], Keeyoung Jung[,§] and Wooyoung Shim*[,†]*

[†] Department of Materials Science and Engineering, Yonsei University, Seoul 03722, Korea
[‡] Department of Materials Science and Engineering, Gyeongsang National University, Jinju 52828, Korea
[§] Materials Research Division, Research Institute of Industrial Science & Technology, Pohang 37673, Korea
[∥] Electrochemical Materials and System Group, Pacific Northwest National Laboratory, Richland, WA 99352, USA

KEYWORDS: Sodium-beta alumina battery, Low- temperature, Liquid metal, Wetting, Bismuth

ABSTRACT: Wetting of the liquid metal on the solid electrolyte of a liquid-metal battery controls the battery's operating temperature and performance. Liquid sodium electrodes are particularly attractive because of their low cost, natural abundance, and geological distribution. But they wet poorly on a solid electrolyte near its melting temperature, limiting their widespread suitability for low-temperature batteries to be used for large-scale energy storage systems. Herein, we develop an isolated metal-island strategy that can improve sodium wetting in sodium-beta alumina batteries that allows operation at lower

temperatures. Our results suggest that *in situ* heat treatment of a solid electrolyte followed by bismuth deposition effectively eliminates oxygen and moisture from the surface of the solid electrolyte, preventing the formation of an oxide layer on the liquid sodium, leading to enhanced wetting. We also show that employing isolated bismuth islands significantly improves cell performance, with cells retaining 94% of their charge after the initial cycle, an improvement over cells without bismuth islands. These results suggest that coating isolated metal islands is a promising and straightforward strategy for the development of low-temperature sodium-beta alumina batteries.

INTRODUCTION

The development of liquid metal batteries is rapidly advancing owing to their high specific energy (energy per unit mass) and high energy density (energy per unit volume), with applications in large-scale stationary electricity storage.[1,2] In particular, significant efforts have been made in sodium-beta alumina batteries (NBBs) having a liquid Na anode and a β''-Al_2O_3 solid electrolyte (BASE),[3–5] which have been employed in large-scale renewable energy storage applications. These efforts have highlighted the importance of battery components, but high temperatures are required for electrochemical activity, impeding the realization of low-temperature NBBs that can avoid costly manufacturing and safety issues.[6,7]

To realize low-temperature NBBs, β''-Al_2O_3 must have a low resistance and sufficient ionic conductivity (0.2–0.4 S/cm at 300 °C) at low operating temperatures. These can be attained by thinning the β''-Al_2O_3 and producing high-quality β''-Al_2O_3 with fewer bulk impurities such as silicon and calcium that form glassy sodium aluminosilicate phases and intergranular calcium aluminate phases, respectively.[8–10] In addition, high ionic conductivity in electrolytes can be

achieved by increasing the volume fraction of the β''-phase in two-phase mixtures (β-Al$_2$O$_3$/β''-Al$_2$O$_3$) via doping with divalent cations such as Mg^{2+}, Ni^{2+}, Zn^{2+}, and Cu^{2+}.[11,12] Ionic conductivity is also affected by the microstructure; for example, larger average grains lead to higher conductivity.[13] Another approach for reducing operating temperatures is to replace β''-Al$_2$O$_3$ with other sodium ion conductors such as glass, glass-ceramic electrolytes (e.g., Na$_3$PS$_4$ glass-ceramic electrolyte),[14] and a NASICON (Na super ionic conductor)-type crystal with the general chemical formula of Na$_{1+x}$Zr$_2$Si$_x$P$_{3-x}$O$_{12}$ ($0 < x < 3$).[5]

Alternatively, improving the wetting behavior of liquid Na on the surface of β''-Al$_2$O$_3$ can produce lower operating-temperature NBBs. Typically, the wetting of liquid Na decreases as temperature decreases, meaning that the active area of the wetting interface between liquid Na and β''-Al$_2$O$_3$ decreases, degrading battery performance.[7] It is well known that poor Na wetting is related to the formation of surface oxidation of the liquid Na when β''-Al$_2$O$_3$ is exposed to moisture-rich conditions (Figure S1),[15,16] necessitating conditioning cycles to reach full cell capacity.[17] To address this wetting problem, additional metal coatings (e.g., Sn, Bi, and In) or porous nanostructures (e.g., Ni nanowires, Pt mesh, and Pb particles) were applied to the surface of β''-Al$_2$O$_3$ to increases the adhesive energy between metal (Na)–metal coating contacts, and to prevent moisture from being absorbed onto the β''-Al$_2$O$_3$.[10,18-21] In addition, the application of various Na alloys with Cs, Sn, and Bi, which have a high work of adhesion (W_{adh}) with β''-Al$_2$O$_3$, have been reported to show improvements in the wetting behavior.[20,22] Taking advantage of this metal passivation effect, this approach, where metal ions are considered potential impurities, causes the problem with Na$^+$ ion transport and limits full utilization of the contact area due to the presence of impurity metals on the surface of the β''-Al$_2$O$_3$.[18,19,23] Therefore, metallic elements that can be alloyed with Na in small amounts must be identified, such that Na$^+$ ion transport is

unimpeded while effectively protecting the surface of the β''-Al$_2$O$_3$, and as a result, removing the need for conditioning cycles.

We have chosen Bi as metallic coating materials, and several important features critical to the choice of Bi, follow: First, Bi can be alloyed with Na as an oxygen getter, such as a Ti or Al sponge,[24,25] to reduce the formation of sodium oxide at the interface and therefore improve wetting. The standard Gibbs free energy of formation of Bi$_2$O$_3$ is -439.0 kJ/mol at 230 °C (compared to -350.8 kJ/mol for Na$_2$O at 230 °C), indicating that Bi$_2$O$_3$ is more likely to be oxidized than Na$_2$O (Table S1), thereby allowing for oxygen getters to prevent formation of sodium oxides on the surface of the liquid Na. Second, the ionic radius of Bi^{3+} is 1.03 Å, which is similar to that of Na$^+$, 1.02 Å (Table S2), and therefore causes less lattice strain at the β''-Al$_2$O$_3$ grain boundary when ion exchange occurs. Previous research has shown that the exchange of Na$^+$ by larger ions such as K$^+$ and Rb$^+$ at 200 °C causes permanent stress such that the β''-Al$_2$O$_3$ fractures.[22] Indeed, when heated to 300 °C, the β''-Al$_2$O$_3$ samples coated with Na-Bi alloys did not fracture (Figure S2), verifying no strong lattice strain was imposed during any ion exchange. Third, a small amount of Bi is completely miscible when alloying with Na, as shown in its binary phase diagram (inset, Figure S3), which ultimately does not interfere with Na transport. For example, the solubility limit of Bi in Na is ~10^{-3}–10^{-2} wt.% at temperatures of < 300 °C (blue dotted line, Figure S3) (log$_{10}$ (at.%Bi) = 7.7169 - 8131.6/T + 1.3774 × 10^6/T^2, (T < 923 K)),[26] which is much lower than that of the alternatives such as Sn, Pb, and Cs. Additionally, Bi is fully soluble in liquid Na at temperatures < 300 °C.[27,28] In this regard, we estimated the upper limit of Bi thin-film thickness for a given volume of liquid Na, where a Na-Bi alloy can form without an excess-Bi thin film on the surface of the β''-Al$_2$O$_3$. The calculated solubility limit of Bi in liquid Na suggests a critical thicknesses t_c of ~10, 46, 152, and 505 nm at temperatures of 150, 200, 250,

and 300 °C, respectively (Figure S4). In addition, we noted that adding Bi (10^{-2} wt.%) to Na did not increase its melting point of 98 °C within detection limits, which would also be beneficial for the potential low-temperature operation of an NBB.

Herein, we describe the improvement of Na wetting behavior on β''-Al_2O_3 that dramatically enhanced battery cell performance. First, we investigated the presence of a kinetically favored Na oxide layer under a moisture-rich environment. It forms quickly but stabilizes thermodynamically, highlighting the necessity of precise control of the water interface on β''-Al_2O_3.[15,23,24] Second, we develop a Bi-island-approach that (i) is impervious to water yet does not interfere with Na conductivity and (ii) improves the Na ion pathway from an electrolyte to the anode on charging. And (iii) as a result, sodium-beta alumina batteries fabricated using our methods can be operated at much lower temperatures than typical NBBs, and without the need for conditioning cycles. Importantly, we found that it was isolated bismuth islands, as opposed to a continuous bismuth film[20], that significantly improves cell performance, retaining 94% charge after the initial cycle. This methodology represents a major advance toward Na wetting engineering, as it provides a protocol to effectively enhance wettability and ultimately leads to improved battery performance.

RESULTS AND DISCUSSION

A single Na-NiCl$_2$ cell consists of a liquid Na (anode)/β''-Al_2O_3 (solid electrolyte)/NiCl$_2$ (cathode) added to a liquid secondary electrolyte (NaAlCl$_4$), with a few-nanometer-sized Bi metal islands deposited on the β''-Al_2O_3. These Bi islands are sandwiched between the anode and electrolyte (Figure 1a). When an Na-NiCl$_2$ cell is typically assembled, a small amount of solid

sodium is applied on the surface of the β''-Al$_2$O$_3$ (anode side), and the anode is almost empty, with a small amount of contact of the sodium with the β''-Al$_2$O$_3$. Upon charging the cell during the first cycle, Na$^+$ ions formed at the cathode diffuse to the anode through the β''-Al$_2$O$_3$ and then fill the empty anode space by one-electron reduction of the Na$^+$ ion. The higher wettability of liquid Na on the surface of β''-Al$_2$O$_3$ induces better charging characteristics, *i.e.*, a low overpotential.[29] In this regard, we utilize two Na filling processes during charging (Figure 1b). First, when Na$^+$ ions diffuse on the β''-Al$_2$O$_3$ surface, they are reduced to liquid Na by accepting electrons from Bi on the anode side of β''-Al$_2$O$_3$ (stage I) and, thus, a strong local active area forms at the edge of the Bi for Na reduction. Second, the significant growth of liquid Na in this active area is expected (stage II) given that the diffusivity of Na$^+$ ion into liquid Na (self-diffusion) is much higher than that into solid Bi (interdiffusion) by a factor of 100–1000 (Figure S5).[30,31] Given that vacancies should be more abundant in the liquid,[32] the activation energy for vacancy diffusion in liquids (Na$^+$ → liquid Na) is lower than that in solids (Na$^+$ → solid Bi) (Figure 1c). This self-diffusion in liquids leads to a large ratio of entropy to enthalpy, and, as a consequence, a lower Gibbs free energy.[32] As a result, further diffusion leads to the conformal filling of the gaps between Bi islands with liquid Na, representing good wetting of liquid Na on the β''-Al$_2$O$_3$ surface (stage III).

Following this concept, we coated the β''-Al$_2$O$_3$ surface with Bi to isolate the β''-Al$_2$O$_3$ surface from moisture (Figure 2a). Briefly, β''-Al$_2$O$_3$ was annealed to 450 °C under a vacuum of ~10^{-8} Torr for 10 h in a sputter chamber to remove possible moisture. Then, a Bi thin film was deposited without breaking vacuum, such that the β''-Al$_2$O$_3$ surface was kept clean and dry, reducing the possibility of forming an oxide layer on the liquid Na. Figure 2b shows representative cross-sectional transmission electron microscopy (TEM) images of the β''-Al$_2$O$_3$

surface in which Bi islands were deposited on the surface. The growth of metal islands on the surface occurred when the cohesive energy (Bi-Bi adatom) exceeded the adhesive energy (Bi-β''-Al$_2$O$_3$). Thus, this occurred when the deposited metal did not fully wet the substrate (contact angle, $\theta > 0$). This growth mode often has been observed in metal-insulator systems.[33] In addition, in the early stage of non-epitaxial Bi deposition, the thin film tends to result in isolated island formation (Cross-sectional TEM and in-plane SEM image of Bi coated β''-Al$_2$O$_3$) Figure S6 and Figure S7). In this manner, we deposited 30-nm-thick Bi islands on a rough β''-Al$_2$O$_3$ surface as in Figure 2b, where the surface was either flat (sub-panel row A and B) or had a trench structure (sub-panel row C). Note that the conformal coating of Bi islands on the surface of the trench was achieved in this magnetron sputtering deposition. The concept of utilizing Bi for passivation, and in particular forming isolated islands, is distinct from previous studies where it was used for thick layers, but continuous metallic films can enhance Na wettability, as follows.

The contact angles for liquid Na on non-preheated and preheated β''-Al$_2$O$_3$ exhibit distinctly different wetting behaviors (Figure S8). For example, in non-preheated β''-Al$_2$O$_3$, an oxide layer on the surface of the liquid Na was observed (top, Figure 3a), which pinned the drop edges to the β''-Al$_2$O$_3$, thus impeding further wetting as the temperature was increased.[23] On the other hand, no obvious oxide layer formed for the preheated β''-Al$_2$O$_3$ (bottom, Figure 3a). In addition, we investigated the manner in which decreasing temperatures affect the contact angle of liquid Na. Figure 3b shows that contact angles decreased from 140° to 80° as the temperature increased from 150 °C to 300 °C for the non-preheated β''-Al$_2$O$_3$, but decreased from 120° at 150 °C to 70° at 300 °C for the preheated β''-Al$_2$O$_3$. Taken together, these data confirm that the surface of β''-Al$_2$O$_3$ must be clean of moisture and oxygen to prevent oxide formation in the experimental environment, such as in a glove box when a sessile drop technique is often used.

Since the surface impurities of β''-Al$_2$O$_3$ cause the contact edges of liquid Na to become pinned by the solid oxide layer,[9] a further reduction in contact angle by completely isolating the surface from moisture- and oxygen-rich environments is advisable and possible.

The wetting properties of liquid Na on Bi-coated β''-Al$_2$O$_3$ at temperatures of 150, 200, 250, and 300 °C in an Ar atmosphere were studied to validate the effects of Bi coating on Na wetting. Compared to the wetting behaviors of preheated (contact angle of 75° at 300 °C) and non-preheated β''-Al$_2$O$_3$ (contact angle of 80° at 300 °C), as shown in Figure 3b, the use of a Na-Bi alloy clearly improves wetting, with a contact angle as low as 60° at 300 °C. These results demonstrate the effectiveness of using a Bi metal coating layer to protect the surface of β''-Al$_2$O$_3$ from moisture while highlighting the potential of Na-Bi alloys to enhance wetting. Note that the contact angle at 150 °C was particularly lower than that at 200 °C (Figure 3b), which is because the Bi thin film (15 nm) was beyond t_c at 150 °C ($t_c \approx 10$ nm), where excess remained in Bi contacts and Na-Bi alloys (red dotted line, Figure S3). That is, a metal (Na-Bi alloy)/metal (remaining Bi thin film) contact resulted in a low Na contact angle. Above 200 °C where the film thickness was less than t_c, no excess Bi thin film was observed on the surface, but instead Bi was completely alloyed with the Na, increasing the contact angle slightly owing to metal (Na-Bi alloy)/ceramic (β''-Al$_2$O$_3$) contact, which is in good agreement with the calculated data (blue dotted line, Figure S3).

These representative examples of Bi-coated structures highlight how the thickness of the Bi coatings are key motifs for wetting experiments (Figure 3c). First, the Bi film thinner than 10 nm does not effectively protect a β''-Al$_2$O$_3$ surface from moisture, such that its contact angle is similar to that of an uncoated β''-Al$_2$O$_3$ surface. Second, as its thickness increases from 10 to 20 nm, where the Bi islands form on the β''-Al$_2$O$_3$ surface, the β''-Al$_2$O$_3$ surface is successfully

isolated from moisture, improving the wetting of the Na (darkened band) at 200 °C. Third, a

thickness over 20 nm exceeds the solubility limit of Bi for Na in our experiments, and a distinct

Na/Bi/β''-Al$_2$O$_3$ interface is maintained. This leads to low contact angles of the Na liquid due to

metal-metal contact between the Na liquid and remaining Bi film. But this is ultimately not

desirable for Na ion transport to β''-Al$_2$O$_3$. In addition, we characterized the Na/Bi/β''-Al$_2$O$_3$

interface above 200 °C, where the Bi film below the critical thickness (< 20 nm) was completely

dissolved into the Na liquid. Local elemental mapping of the Na/Bi/β''-Al$_2$O$_3$ interface by energy

dispersive x-ray spectroscopy (EDS) was performed to probe compositional variations across the

interface (Figure 3d). Cross-sectional elemental maps show that the Bi film below 20 nm, within

the equilibrium solubility limit of Bi for Na, was completely dissolved into the Na liquid (middle,

Figure 3d), while in the 100-nm Bi film, which is over the solubility limit, appeared localized in

the interface region (right, Figure 3d). Note that quantitative analysis of Na, Bi, and Al

composition variation, however, shows that the interface was not atomically abrupt but rather

broadly transitioned over a length scale of a few microns. To provide fundamental insight into

the mixing of dissolved Bi in Na, *ab initio* density-functional theory (DFT) calculations were

performed, and the thermodynamics of the Na–Bi alloy system were investigated with the aid of

the energy convex hull diagram (Figure S9). Under the dilute concentration of Bi in Na, we

found that the dissolved Bi atom tends to form the thermodynamically most stable alloy structure,

Na$_3$Bi (bottom-left image, Figure 3d), with a negative formation energy of -0.40 eV/atom. On the

other hand, NaBi was found to be stabilized with a negative formation energy of -0.33eV/atom

as the Bi concentration was increased to reach the 1:1 molar ratio to Na.

 Along with its wetting behavior, we also explored the electrical transport of Na ions to

investigate its effect on the Bi coating. Two-point probe measurements of the Bi-coated β''-Al$_2$O$_3$

surface were used to measure conductivity as a function of temperature (Figure S10a). We prepared Bi-coated samples 2.8 cm^2 in area and 2.03 mm thick (Figure S10b). Electrochemical impedance spectra were measured in the temperature range of 175 to 300 °C for bare (Figure 4a) and Bi-coated β''-Al$_2$O$_3$ (Figure 4b). During the first cycle, heating from 175 to 300 °C, ohmic behavior was dominant in both cases. In our study, the measured total resistance (R_{tot}), the sum of ohmic and polarization resistances, can be analyzed in terms of a change in the contact area and the condition of the interface between the liquid Na and β''-Al$_2$O$_3$. We focused on the former case since the ohmic resistance, R_{Ohm}, varied by contact area. The use of R_{Ohm} simplified the identification of the effect of the Bi coating on wetting behavior as a factor in varying the active area. It is primarily determined by the bulk properties, *i.e.*, the ionic conductivity, of β''-Al$_2$O$_3$ that are relevant to size (area/length), whereas polarization resistance is influenced by parasitic effects that disturb ionic transport at the interface. When the interface is clean (*e.g.*, no parasitic capacitance), a change in contact area is mostly responsible for R_{Ohm} and, thus, strong wetting-conductivity coupling will occur. The difference in wetting-conductivity coupling for Bi-coated and bare β''-Al$_2$O$_3$ yields different conductances for varying temperatures, where the R_{Ohm} shifts between samples can be analyzed in terms of the different degree of wetting. Indeed, Figure 4a shows that R_{Ohm} decreased to 10.4, 5.8, 3.4, 2.0, and 0.8 Ω at temperatures of 175, 200, 225, 250, and 300 °C, respectively, for a bare β''-Al$_2$O$_3$, while Figure 4b shows R_{Ohm} for the Bi-coated β''-Al$_2$O$_3$ at temperatures of 175, 200, 225, 250, and 300 °C were 3.0, 2.2, 1.7, 1.4, and 1.0 Ω, respectively. The contact angle of the liquid droplet, therefore, decreased such that the wetting of the liquid Na was enhanced, increasing the contact area at the interface. Therefore, a decrease in R_{Ohm} resulted from an increased contact area, which was in turn caused by the improved wetting by the Bi coating.

Figures 4c and 4d show the Arrhenius plots of the ionic conductivities of the bare and Bi-coated β''-Al$_2$O$_3$, respectively. The conductivity of the Bi-coated β''-Al$_2$O$_3$ was higher than that of bare β''-Al$_2$O$_3$ for all cycles and at all measured temperatures, highlighting the improved wetting with the Bi coating. During the first cycle, the conductivity difference was more prominently observed at lower temperatures, and this enhanced conductivity represents enhanced wetting behavior compared to bare β''-Al$_2$O$_3$ (Figure 4c). For example, the conductivities of the bare and Bi-coated samples, σ_{bare} and σ_{Bi}, were 6.88×10^{-3} and 2.09×10^{-2} S/cm at 175 °C, respectively, indicating that the Bi coating induced a 3 times larger active area than that of the bare surface. In addition, in the second cycle a significant conductivity increase was observed in σ_{bare}, to 1.50×10^{-2} S/cm at 175 °C, while no significant change was observed in σ_{Bi}. This is because wetting had already been initiated during the first cycle for the bare β''-Al$_2$O$_3$, which increased subsequent wetting. For the Bi-coated sample, on the other hand, this initiation was not necessarily required since the wetting during the first cycle was already sufficient, in the sense that no impurities resided on the surface impeding the wettability. Indeed, we found that after many cycles σ_{Bi} remained stable (Figure 4e).

We characterized the charge/discharge behavior of Na-NiCl$_2$ cells (Figure S11) to investigate the effect of the Bi coating at 175 °C. Three different surface modifications of the anode sides of the β''-Al$_2$O$_3$ were made: bare β''-Al$_2$O$_3$, Bi-coated β''-Al$_2$O$_3$, and scratched Bi-coated β''-Al$_2$O$_3$ (Figure S12). The scratched Bi-coated β''-Al$_2$O$_3$ was prepared by scratching the Bi film with a diamond cutter in a glove box (H$_2$O, O$_2$ below 1 ppm) to prevent further exposure to ambient moisture. Na-NiCl$_2$ batteries were assembled in their discharged states. Some liquid Na initially resided in the anode for the electrical contact with β''-Al$_2$O$_3$ and began the charge cycle where Na$^+$ ions were transported from cathode to anode.[34] In this sense, the scratched Bi

film increased the active area (edge of Bi islands) and the Na$^+$ ion path across the interface of the Bi and β''-Al$_2$O$_3$ (Figure 5a).

Typically, Na-NiCl$_2$ batteries require conditioning cycles to properly activate them, due to the poor initial Na wetting during low temperature operation below 200 °C. To investigate the initial wetting performance of cells, the voltage profiles of the initial cycle are compared in Figure 5b. In this measurement, a cutoff voltage of 2.8 V (for charging) was selected based on the fact that, when the cell was overcharged higher than 2.8 V, an undesirable side reaction between Ni and NaAlCl$_4$ catholyte is known to occur.[22] If the cell was overdischarged below a state of charge (SOC) lower than 20% (~2.4 V), a small amount of Na would remain in the anode chamber, possibly leading to high cell resistance because insufficient Na was available to provide electrical contact between Na and the β''-Al$_2$O$_3$.[22] Note that the presence of a plateau region during the charge/discharge processes indicates the oxidation of Ni to NiCl$_2$, and reduction of NiCl$_2$ to Ni,[17,34] respectively, for the initial cycle and as a result of the electrochemical reactions in the Na-NiCl$_2$ cell. For example, such a plateau was clearly observed for the Bi-coated (blue curve) and scratched Bi-coated β''-Al$_2$O$_3$ (red curve), but was not observed in the bare β''-Al$_2$O$_3$ cell (Figure 5b, black). This implies that reversible electrochemical reactions occurred in both Bi-treated cells even during the initial cycle. Indeed, we found that the scratched Bi-coated β''-Al$_2$O$_3$ and Bi-coated β''-Al$_2$O$_3$ cells were charged to 94% and 48% of the SOC, but the bare β''-Al$_2$O$_3$ cell was not activated during the initial cycle and required many cycles (26 cycles) for activation (100% charging, Figure S13) because of its high overpotential due to poor wetting and inefficient utilization of the cathode materials.

These results clearly demonstrate that excellent initial wetting was achieved in Na-NiCl$_2$ cells with Bi-coated β''-Al$_2$O$_3$, just as in the higher Na$^+$-ion conductivity of the Bi-coated sample

shown in Figure 4c. The capacity of the scratched Bi-coated sample (148 mAh) was higher than that of the Bi-coated (75 mAh) sample, due to the increased Na ion path (Figure 5a). In addition, during the cycling test (Figure 5c) with a constant current of 5 mA (1.7 mA/cm^2) and a cutoff voltage between 2.4 and 2.8 V, Bi-coated and scratched Bi-coated β''-Al$_2$O$_3$ cells had relatively stable cycles, in contrast to the bare cell. Figure 5d shows cross-sectional high-angle annular dark-field-scanning TEM- (HAADF-STEM) images and EDS elemental maps of the β''-Al$_2$O$_3$ surface, showing as-deposited Bi islands (upper row) and the β''-Al$_2$O$_3$ surface-scratched Bi islands (bottom row). The as-deposited Bi islands (thickness ~30 nm) were crushed into smaller discrete islands of a few-nm with smaller gaps between islands. In this sense, the scratched Bi coating may have increased surface area supporting Na transport across the interface of the Bi and β''-Al$_2$O$_3$, providing a simple approach for tuning liquid Na wettability and cell stability at the low temperature of 175 °C (Figure S14).

CONCLUSION

These studies demonstrate that coating Bi on the β''-Al$_2$O$_3$ surface of an NBB can effectively enhance the wetting of liquid Na and cell performance, thus providing a facile approach for realizing low temperature NBBs. Compared to a bare β''-Al$_2$O$_3$ electrolyte, the Bi coating, which takes advantage of bismuth's similar ionic radius, lower solubility limit, and higher oxide formation energy than those of Na. This provides greater cell reaction performance during charge/discharge cycling and thereby stabilizes the cells of Na-NiCl$_2$ batteries. In addition, simple thin-film deposition offers a practical cell fabrication approach, and shows substantial promise for large-scale production. However, Na-NiCl$_2$ battery cycling performance must be further improved by addressing several issues that include (i) the loss of Na$^+$ ion conductivity of

β''-Al$_2$O$_3$ during cycling (Figure 4e), which is due to a possible calcium impurity (Figure S15) in β''-Al$_2$O$_3$ that migrates to the Na/β''-Al$_2$O$_3$ or the Bi film/β''-Al$_2$O$_3$ interfaces to form an oxide film;[9] (ii) the loss of capacity during cycling (Figure 5c), which is due to the formation of a thicker NiCl$_2$ layer on the Ni surface during charge cycling that limits cell capacity;[17,35] and (iii) the potential solubility of NiCl$_2$ in a NaAlCl$_4$ catholyte that causes an exchange of Ni and Na ions in β''-Al$_2$O$_3$.[7] Although a simple methodology for fabricating batteries is unlikely to offer highly competitive cell performance, a Bi coating on the β''-Al$_2$O$_3$ solid electrolyte will be useful in the development of robust, stable, low-temperature NBBs.

METHODS

Bi coating. The β''-Al$_2$O$_3$ was annealed to 450 °C under a vacuum of ~10^{-8} Torr for 10 h in a chamber to remove possible moisture, after which a Bi thin film was sputter-deposited without breaking vacuum. Bi thin films were deposited on the β''-Al$_2$O$_3$ surface in a DC magnetron sputtering system with a base pressure of ~10^{-8} Torr and a working pressure of 2.3 mTorr with an Ar flow of 34 sccm. The coatings were deposited from a 2-inch Bi (99.99%) target in an Ar (99.999%) atmosphere. The distance from substrate to target was 10 cm. The Bi films were deposited at 10~100 nm at a rate of 0.48 nm/s at room temperature. The discharge power was 10 W. The thickness of the coatings deposited on the β''-Al$_2$O$_3$ was measured using a field-emission scanning electron microscopy, JEOL-7001F, and by cross-sectional transmission electron microscopy, JEM-ARM 200F (JEOL, USA).

Wetting test. The contact angle of the liquid Na on the β''-Al$_2$O$_3$ surface was measured by a sessile drop technique in an Ar-protected glove box. High-purity Na (99.9%) was used and heated to the measurement temperature in an alumina crucible by a hot plate. Drops of Na were

transferred to the β''-Al$_2$O$_3$ surface using a glass syringe. Bare β''-Al$_2$O$_3$ samples were preheated or not preheated to the measurement temperature in a quartz tube chamber which is surrounded by a Kanthal tube furnace (Figure S16). Some β''-Al$_2$O$_3$ samples were heated to 450 °C in a high vacuum (~10^{-8} Torr) sputter chamber for 10 h and continuously coated with Bi at room temperature in the same chamber. The temperature range of the wetting test was 150 to 300 °C and the duration after transference of the Na droplets to the β''-Al$_2$O$_3$ surface for wetting angle measurements was 30 min. Angle measurement was performed in a glove box by a CCD camera and the SEO surfaceware9 program, which provides an instant contact angle (Figure S17).

Characterization. Cross-section analysis of the Na on Bi-coated β''-Al$_2$O$_3$ was performed using a JIB-4601F focused ion beam (FIB)/field emission-SEM dual-beam system (JEOL, USA). This was done under high vacuum because Na is highly reactive in moisture and air. After preparing the cross-section, local elemental mapping of Na/Bi/β''-Al$_2$O$_3$ was performed by energy dispersive x-ray spectroscopy. The cross-sectional TEM sample of Bi/β''-Al$_2$O$_3$ was also prepared using FIB. To prevent damage from the Ga$^+$ ion beam, the Bi/β''-Al$_2$O$_3$ substrate was coated with a carbon layer. STEM EDS elemental mapping was performed using a JEM-ARM 200F (JEOL, USA).

Conductivity measurement. The electro-chemical impedance spectra of the Na/β''-Al$_2$O$_3$/Na cell were obtained in the frequency range from 0.1 Hz to 200 kHz at an amplitude of 0.1 V with a potentiostat (HP803, BioLogic, France) as a function of temperature in the range of 150 to 300 °C. We used bare and one-side Bi-coated β''-Al$_2$O$_3$ (Figure S10).

Cell assembly. Detailed methods for cathode material preparation and the planar cell assembly procedure have been reported previously.[35] The planar cell consisted of battery cases for the cathode and anode, an α-Al$_2$O$_3$ fixture, a β''-Al$_2$O$_3$ disc (INOTEC, 3 cm^2 active area) and

current collectors (Mo foil for the cathode and stainless steel shim for the anode) between the electrode end-cap and electrode. A schematic of the planar cell used in this work is shown in Figure S11. The β''-Al$_2$O$_3$ discs were glass-sealed in an α-Al$_2$O$_3$ fixture to separate cathode and anode chambers. The β''-Al$_2$O$_3$ discs were used in bare and surface-treated states on the anode side of β''-Al$_2$O$_3$ discs. Two different surface treatments were conducted. In one, β''-Al$_2$O$_3$ discs were annealed to 450 °C under a vacuum of ~10^{-8} Torr for 10 h in a sputter chamber, and then a Bi thin film (15 nm) was deposited without breaking the vacuum. One film was scratched in all directions by a diamond scribe in the glove box (H$_2$O, O$_2$ <1 ppm). The planar cell was assembled in a discharged state. The ~1 g of cathode granules comprising Ni (Novamet, Type 255) and NaCl (Alfa Aesar, 99.99%) with a molar ratio of Ni to NaCl = 1.82, were placed into the cathode chamber with cathode additives, and then NaAlCl$_4$, the secondary electrolyte was vacuum-infiltrated into the granules. A small amount of metallic Na (< 5 mg) was added on the surface of the β''-Al$_2$O$_3$ (anode side) for an initial electrical contact. The entire cell assembly procedure was conducted in a glove box. The specific capacity of the planar cell in this work was 157 mAh/g without considering the mass of the melt, NaAlCl$_4$ (Table S3).

Cell tests. The assembled Na-NiCl$_2$ cells were moved from the glove box into furnaces for battery cycle tests in air. The performance of cells with bare β''-Al$_2$O$_3$, Bi-coated β''-Al$_2$O$_3$, and scratched Bi-coated β''-Al$_2$O$_3$ were compared at 175 °C. Cell tests were performed using an Arbin potentiostat (MSTAT 8000) controlled by vendor-supplied software (MITS Pro). The cells were tested in two different current modes – first and regular cycles. We intentionally and sequentially increased currents for initial charging. For example, for the Bi-coated case, 0.6 mA (for 2 h), 1 mA (for 10 h), 2 mA (for 17 h), 4 mA (for 4 h), and 5 mA (until the cell voltage reached 2.8 V) was used. We started with a relatively low current because the cell was assembled

in its discharged state, where the amount of liquid sodium in the anode chamber was very small and thus led to a high electrical resistance. High current can lead to high over-potential in initial charging. After the first cycle, the cells were charged and discharged by a constant current of 5 mA and cutoff voltages between 2.4 V (discharge) and 2.8 V (charge). For the bare and scratched Bi-coated case, testing was again in order of increasing current: 0.6 mA (for 2 h), 1 mA (for 10 h), and 5 mA (until the cell voltage reached 2.8 V). After the initial cycle, the cells were charged and discharged by a constant current of 5 mA.

Computational methodology. All density-functional theory (DFT) calculations were performed with the projector-augmented wave (PAW) method as implemented in the Vienna *Ab initio* Simulation Package (VASP).[36–38] Self-consistent, van der Waals-corrected, semi-local type exchange-correlation functions (optB86b-vdW) were used,[39] with a plane-wave kinetic energy cutoff of 300 eV. The reciprocal space integration was under the Γ-centered k-point grid with 0.2 Å between each reciprocal point. For the geometrical relaxation of the structures, atomic positions were relaxed until the forces acting on the atoms were <0.02 eV/Å. The convex hull of each Bi-Na configuration was obtained from the Open Quantum Materials Database (OQMD).[40,41] Formation energy (E_{form}) is defined as $E_{form} = \frac{E_{tot} - N_{Na} * E_{Na} - N_{Bi} * E_{Bi}}{N_{Na} + N_{Bi}}$, where E_{tot}, E_{Na}, E_{Bi}, N_{Na} and N_{Bi} denote total energy of the system, bulk Na, bulk Bi, number of Na atoms, and number of Bi atoms, respectively.

ASSOCIATED CONTENT

Supporting Information

Additional details of experimental results: a detailed process of the Bi coating, solubility of Bi in liquid Na, wetting test, DFT-calculated energy convex hull of Na-Bi system, two-point probe measurements, structure of the planar cell, SEM images and schematics of the samples, additional charge-discharge experimental results, Ca contents in β''-Al_2O_3, Gibbs free energies of formation meal oxides, and ionic radii of metal ions (PDF)

AUTHOR INFORMATION

Corresponding Author

* E-mail: keeyoung.jung@rist.re.kr

* E-mail: wshim@yonsei.ac.kr.

NOTES

The authors declare no competing financial interest.

ACKNOWLEDGMENT

REFERENCES

(1) Kim, H.; Boysen, D. A.; Newhouse, J. M.; Spatocco, B. L.; Chung, B.; Burke, P. J.; Bradwell, D. J.; Jiang, K.; Tomaszowska, A. A.; Wang, K.; Wei, W.; Ortiz, L. A.; Barriga, S. A.; Poizeau, S. M.; Sadoway, D. R. Liquid Metal Batteries: Past, Present, and Future. *Chem. Rev.* **2013**, *113,* 2075-2099.

(2) Yang, Z.; Zhang, J.; Kinter-Meyer, M. C. W.; Lu, X.; Choi, D.; Lemmon, J. P.; Liu, J. Electrochemical Energy Storage for Green Grid. *Chem. Rev.* **2011**, *111,* 3577-3613.

(3) Wen, Z.; Hu, Y.; Wu, X.; Han, J.; Gu, Z. Main Challenges for High Performance NAS Battery: Materials and Interfaces. *Adv. Funct. Mater.* **2013**, *23*, 1005-1018.

(4) Lu, X.; Xia, G.; Lemmon, J. P.; Yang, Z. Advanced materials for sodium-beta alumina batteries: Status, challenges and perspectives. *J. Power Sources* **2010**, *195*, 2431-2442.

(5) Hueso, K. B.; Armand, M.; Rojo, T. High temperature sodium batteries: status, challenges and future trends. *Energy Environ*. Sci. **2013**, *6*, 734-749.

(6) Chang, H. J.; Lu, X.; Bonnett, J. F.; Canfield, N. L.; Son, S.; Park, Y. C.; Jung, K. Y.; Sprenkle, V. L.; Li, G. Development of intermediate temperature sodium nickel chloride rechargeable batteries using conventional polymer sealing technologies. *J. Power Sources* **2017**, *348*, 150-157.

(7) Lu, X.; Li, G.; Kim, J. Y.; Lemmon, J. P.; Sprenkle, V. L.; Yang, Z. The effects of temperature on the electrochemical performance of sodium-nickel chloride batteries. *J. Power Sources* **2012**, *215*, 288-295.

(8)   Wei, X. L.; Xia, Y.; Liu, X. M.; Yang, H.; Shen, X. D. Preparation of Sodium beta''-alumina electrolyte thin film by electrophoretic deposition using Taguchi experimental design approach. *Electrochim. Acta* **2014**, *136*, 250-256.

(9)   Yasui, I.; Doremus, R. H. Effects of Calcium, Potassium, and Iron Ions on Degradation of *β''*-Alumina. *J. Electrochem. Soc*. **1978**, *125*, 1007-1010.

(10) Hu, Y.; Wen, Z.; Wu, X.; Lu, Y. Nickel nanowire network coating to alleviate interfacial polarization for Na-beta battery applications. *J. Power Sources* **2013**, *240*, 786-795.

(11) Imai, A.; Harata, M. Ionic Conduction of Impurity-Doped *β*-Alumina Ceramics. Jpn. *J. Appl. Phys.* **1972**, *11*, 180-185.

(12) Zhu, C.; Xue, J. Structure and properties relationships of beta-Al_2O_3 electrolyte materials. *J. Alloys compd.* **2012**, *517*, 182-185.

(13) Dunn, B.; Kamath, H.; Tarascon, J. M. Electrical Energy Storage for the Grid: A Battery of Choices. *Science* **2011**, *334*, 928-935.

(14) Hayashi, A.; Noi, K.; Sakuda, A.; Tatsumisago, M. Superionic glass-ceramic electrolytes for room-temperature rechargeable sodium batteries. *Nat. Commun.* **2012**, *3*, 856-860.

(15) Viswanathan, L.; Virkar, A. V. Wetting characteristics of sodium on *β''*- alumina and on nasicon. *J. Mater. Sci.* **1982**, *17*, 753-759.

(16) Marini, A.; Flor, G.; Massarotti, V.; McGhie, A. R.; Farrington, G. C. Hydration and carbonation of Beta alumina powders. *J. Electrochem. Soc.* **1985**, *132*, 1250-1254.

(17) Chang, H. J.; Canfield, N. L.; Jung, K.; Sprenkle, V. L.; Li, G. Advanced Na-NiCl2 Battery Using Nickel-Coated Graphite with Core-Shell Microarchitecture. *ACS Appl, Mater. Interfaces* **2017**, *9*, 11609-11614

(18) Reed, D.; Coffey, G.; Mast, E.; Canfield, N.; Mansurov, J.; Lu, X.; Sprenkle, V. Wetting of sodium on β''-Al_2O_3/YSZ composites for low temperature planar sodium-metal hide batteries. *J. Power Sources* **2013**, *227*, 94-100.

(19) Li, G.; Lu, X.; Kim, J. Y.; Lemmon, J. P.; Sprenkle, V. L. Improved cycling behavior of ZEBRA battery operated at intermediate temperature of 175 °C. *J. Power Sources* **2014**, *249*, 414-417.

(20) Ahlbrecht, K.; Bucharsky, C.; Holzapfel, M.; Tüvke, J.; Hoffmann, M. J. Investigation of the wetting behavior of Na and Na alloys on uncoated and coated Na-β''-alumina at temperatures below 150 °C. *Ionics* **2017**, *23*, 1319-1327.

(21) Hee-Jung, C.; Xiaochuan, L.; Jeffery, F. B.; Nathan, L. C.; Keesung, H.; Mark, H. E.; Keeyoung, J.; Vicent, L. S.; Guosheng, L. Decorating β″-alumina solid-state electrolytes with micron Pb spherical particles for improving Na wettability at lower temperatures. *J. Mater. Chem. A* **2018**, *6*, 19703-19711.

(22) Lu, X.; Li, G.; Kim, J. Y.; Mei, D.; Lemmon, J. P.; Sprenkle, V. L.; Liu, J. Liquid-metal electrode to enable ultra-low temperature sodium-beta alumina batteries for renewable energy storage. *Nat. Commun.* **2014**, *5*, 4578-4585.

(23) Sobczak, N.; Singh, M.; Asthana, R. High-temperature wettability measurements in metal/ceramic systems – Some methodological issues. Curr. Opin. *Solid State Mater. Sci.* **2005**, *9*, 241-253.

(24) Williams, D. D.; Grand, J. A.; Miller, R. R. Determination of the solubility of oxygen bearing impurities in sodium, potassium and their alloys. *J. Phys. Chem.* **1959**, *63*, 68-70.

(25) Naito, K.; Tsuji, T.; Matsui, T.; Une, K. Purification of Inert Gas: Removal of Oxygen with a Metallic Getter. *J. Nucl. Sci. Technol.* **1974**, *11*, 22-28.

(26) Sangster, J.; Pelton, A. D. The Bi-Na (Bismuth-Sodium) System. *J. Phase Equilib.* **1991**, *12*, 451-456.

(27) Bale, C. W. The Cs-Na (Cesium-Sodium) System. *Bulletin of Alloy Phase Diagrams* **1982**, *3*, 310-313.

(28) Hubberstey, P.; Pulham, R. J. Solubility of Tin and Germanium in Liquid Sodium: The Sodium-Tin Partial Phase Diagram. *J. Chem. Soc. Dalton Trans.* **1974**, *14*, 1541-1544.

(29) Guosheng, L.; Xiaochuan, L.; Jin, Y. K.; Kerry, D. M.; Hee Jung, C.; Nathan, L. C.; Vincent, L. S. Advanced intermediate temperature sodium-nickel chloride batteries with ultra-high energy density. *Nat. Commun.* **2016**, 7, 10683-10688.

(30) Yuan, J. Y.; Ming, Z. Q.; Zheng, G. Z.; Fu, J. G. Molecular dynamics simulation of self-diffusion coefficients for liquid metals. *Chin. Phys. B* **2013**, *22*, 083101

(31) Qian, G. X.; Weinert, M.; Fernando, G.W.; Davenport, J. W. First-Principles Calculation of the Activation Energy for Diffusion in Liquid Sodium. *Phys. Rev. Lett.* **1990**, *64*, 1146-1149

(32) Eyring, H.; Ree, T. Significant Liquid Structures, VI. The Vacancy theory of Liquids. *Proc. Nat. Acad. Sci. U.S.* **1961**, *47*, 526-537

(33) Ohring, M. *The Materials Science of Thin Films*, Wiley, Academic Press, London, UK **1992**.

(34) Li, G.; Lu, X.; Kim, J. Y.; Engelhard, M. H.; Lemmon, J. P.; Sprenkle, V. L. The role of FeS in initial activation and performance degradation of Na-NiCl$_2$ batteries. *J. Power Sources* **2014**, *272*, 398-403

(35) Li, G.; Lu, X.; Kim, J. Y.; Lemmon, J. P.; Sprenkle, V. L. Cell degradation of a Na-NiCl$_2$ (ZEBRA) battery. *J. Mater.* Chem. A **2013**, *1*, 14935-14942

(36) Kresse, G.; Hafner, J.; Ab initio molecular dynamics for liquid metals. *Phys. Rev. B* **1993**, *47*, 558-561

(37) Kresse, G.; Hafner, J. Ab initio molecular-dynamics simulation of the liquid-metal-amorphous-semiconductor transition in germanium. *Phys. Rev. B* **1994**, *49*, 14251-14269

(38) Kresse, G.; Furthmüller, J. Efficient iterative schemes for ab initio total-energy calculations using a plane-wave basis set. *Phys. Rev. B* **1996**, *54*, 11169-11186

(39) Klimeš, J.; Bowler, D. R.; Michaelides, A. Van der Waals density functionals applied to solids. *Phys. Rev. B* **2011**, *83*, 195131

(40) Saal, J. E.; Kirklin, S.; Aykol, M.; Meredig, B.; Wolverton, C. Materials Design and Discovery with High-Throughput density Fuctional Theory: The Open Quantum Materials Database. *JOM* **2013**, *65*, 1501-1509

(41) Kirklin, S.; Saal, J. E.; Meredig, B.; Thompson, A.; Doak, J. W.; Aykol ,M.; Rühl, S.; Wolverton, C. The Open Quantum Materials Database (OQMD): assessing the accuracy of DFT. *npj Computational Materials* **2015**, *1*, 15010.

(42) Dawei, S.; Shixue, D.; Guoxiu, W. Bismuth: A new anode for the Na-ion battery. *Nano Energy* **2015**, *12*, 88-95.
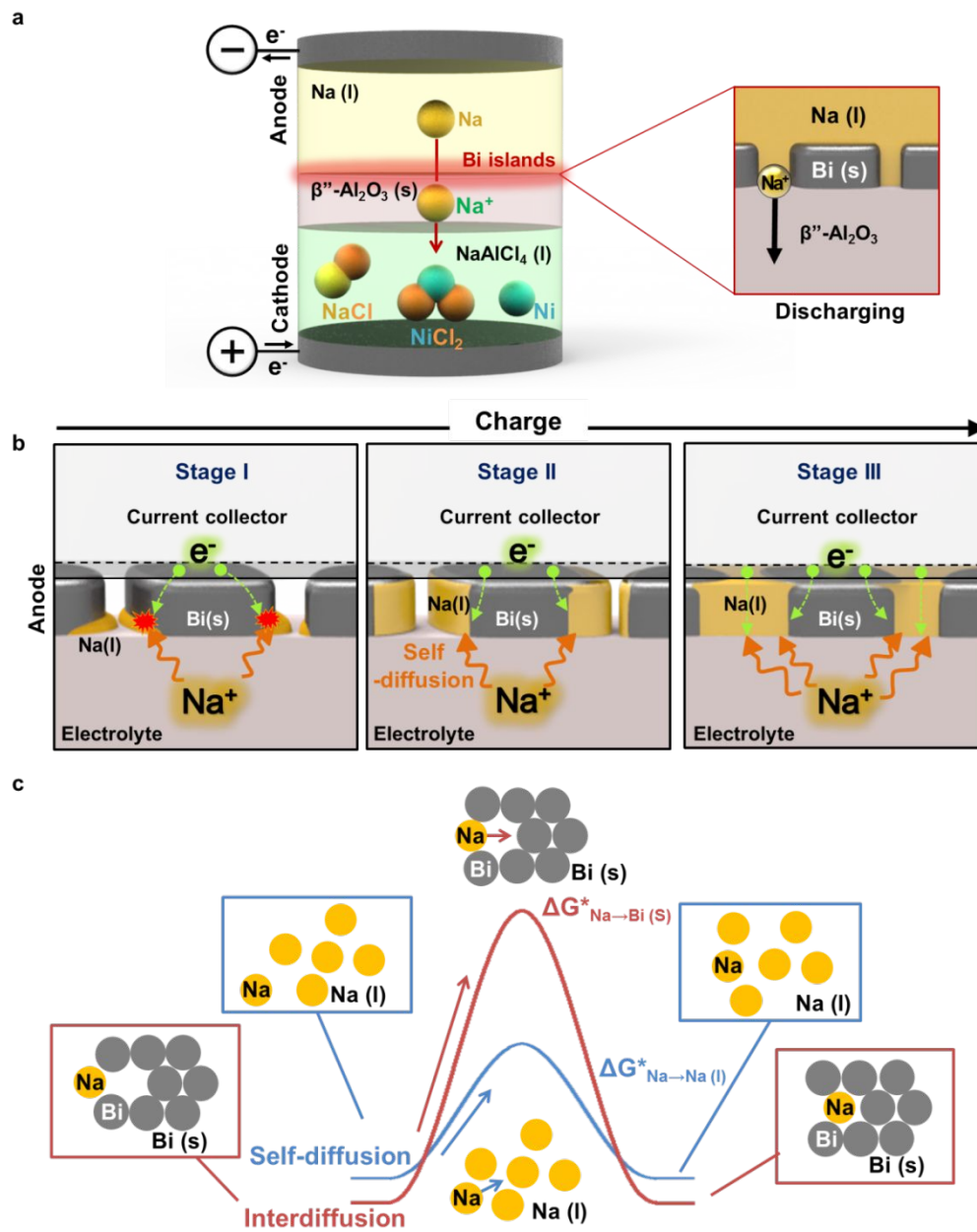
Figure 1. a) Schematic of the Na-NiCl$_2$ cell. b) Na filling process of Bi-coated β''-Al$_2$O$_3$ cell upon charging. c) Schematic of activation energies of diffusion in liquid Na and solid Bi.
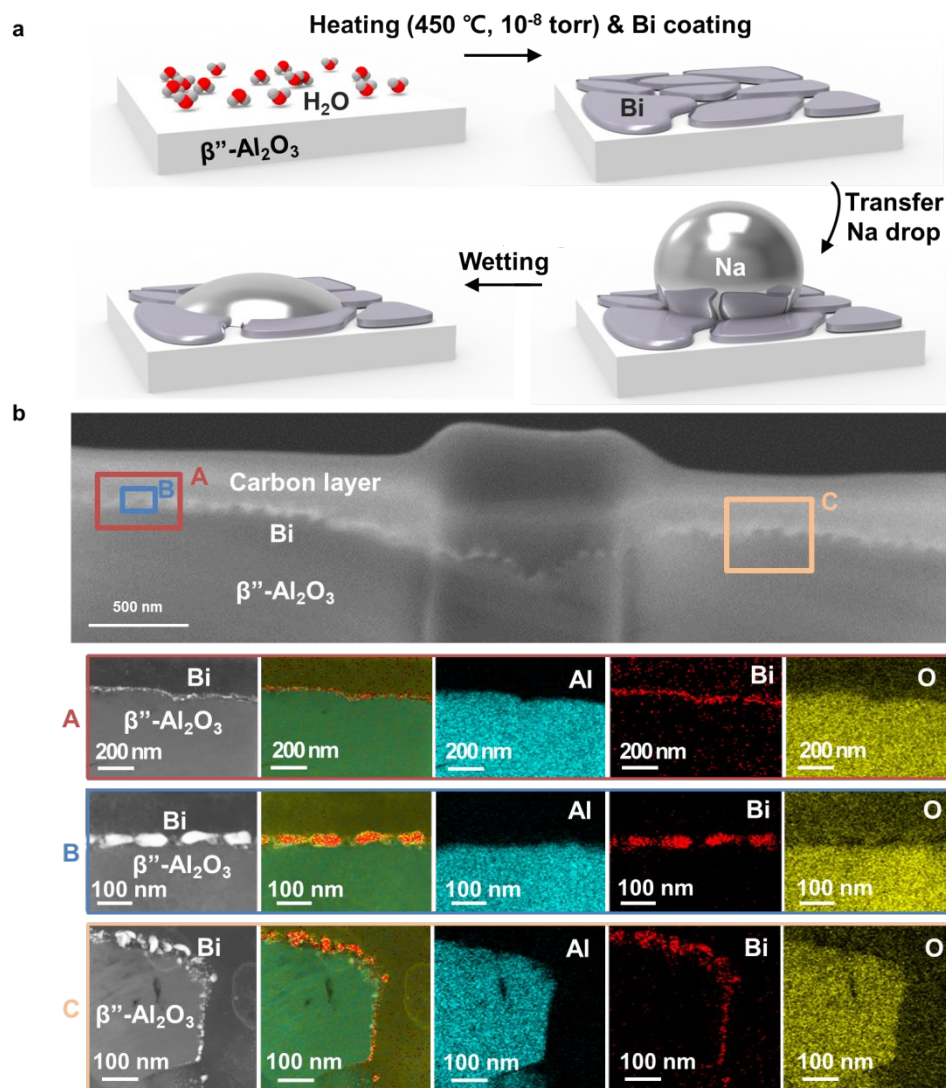
Figure 2. a) Process of surface cleaning and formation of the metal thin-film protection layer. The surface of β''-Al$_2$O$_3$ was cleaned by annealing. Thin films of β''-Al$_2$O$_3$ and Bi were deposited by sputtering, followed by the liquid Na wetting test on the surface of β''-Al$_2$O$_3$. b) Cross-sectional TEM image and high-resolution EDS elemental mapping of the β''-Al$_2$O$_3$ surface where Bi islands were deposited. To prevent damage from the Ga$^+$ ion beam during FIB sample preparation, a carbon layer was coated on the Bi film. Columns in (b) represent a TEM image of the mapped area, the composite chemical map, and maps of Al, Bi, and O, respectively.
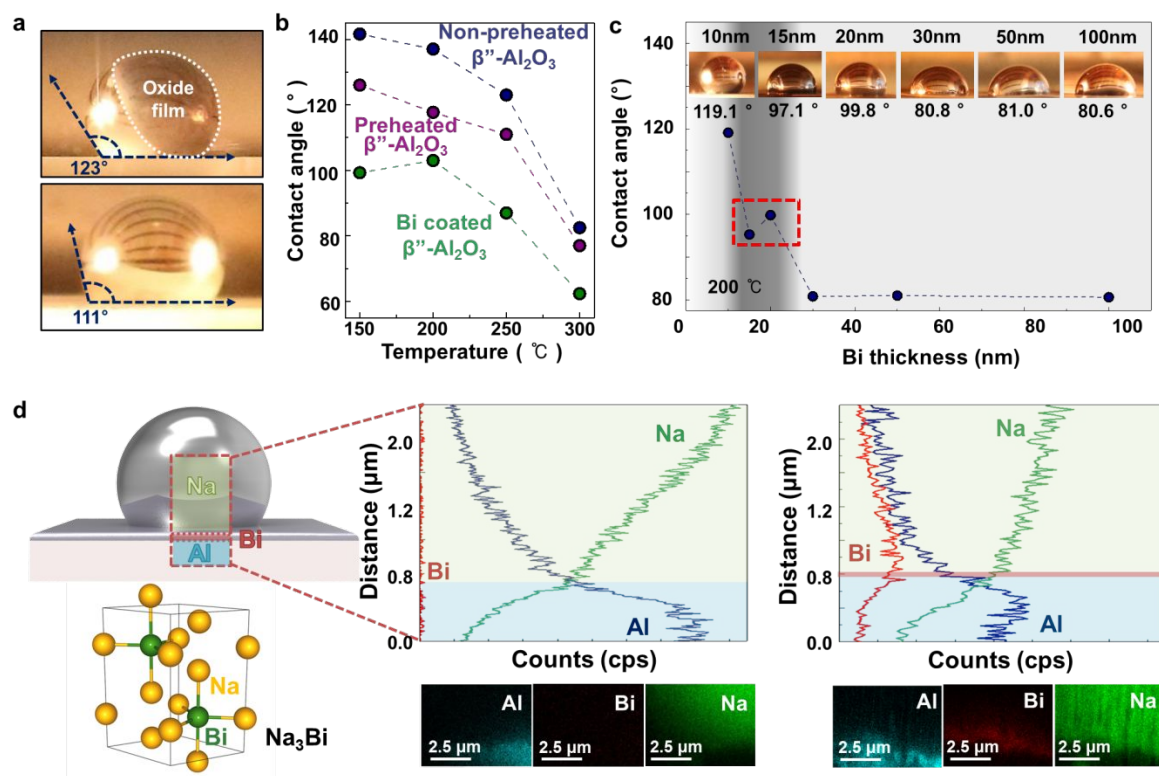
Figure 3. a) Photograph of Na droplet on the non-preheated β''-Al$_2$O$_3$ at 250 °C with an oxide layer of the surface (top) and Na droplet on the preheated β''-Al$_2$O$_3$ (bottom). b) Contact angle change on the preheated, non-preheated and Bi-coated β''-Al$_2$O$_3$ with increasing temperature. c) Contact-angle change at 200 °C due to the Bi film thickness. d) Schematic of the sampled region (red dotted box) and SEM/EDS line scans and mapping across the Na-Bi alloy/β''-Al$_2$O$_3$ interface in the sample with the Bi film below the critical thickness (< 30 nm, left) and with a Bi film of Bi (100 nm, right).

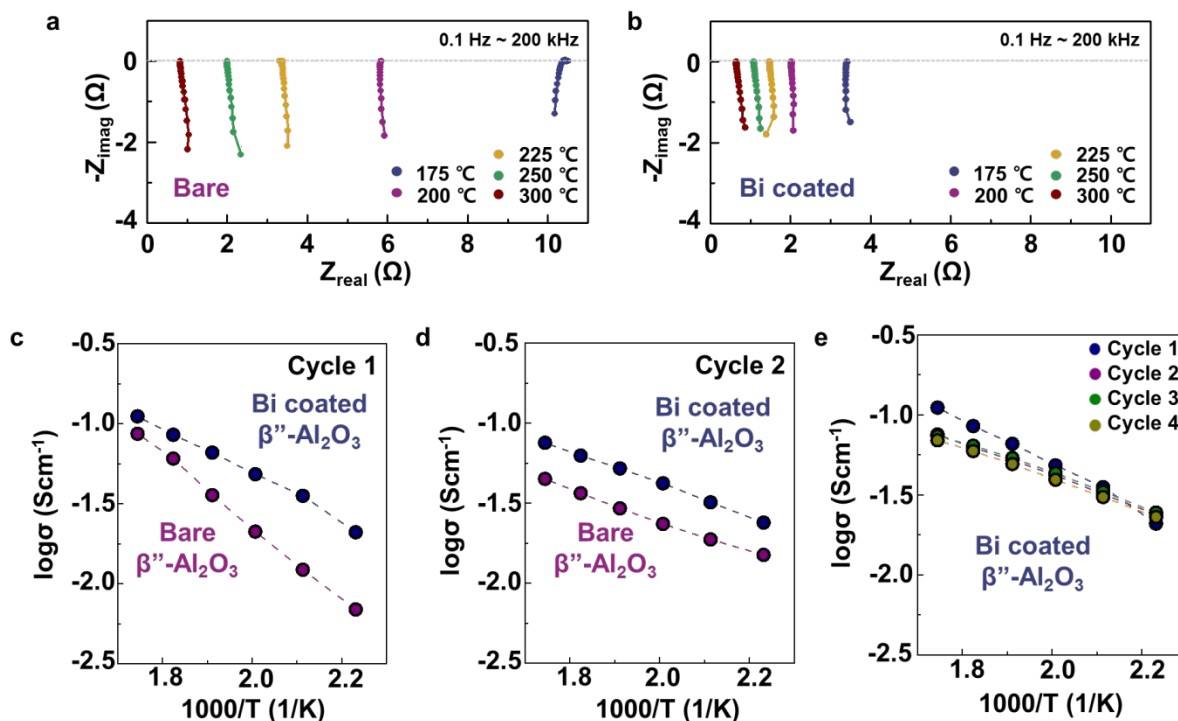**Figure 4.** a) EIS spectra of bare β''-Al$_2$O$_3$. b) EIS spectra of Bi-coated β''-Al$_2$O$_3$. c) Arrhenius plot (AC) of the Na$^+$ ion conductivities of bare and Bi-coated β''-Al$_2$O$_3$ at each temperature during the cycle 1. d) Arrhenius plot (AC) of the Na$^+$ ion conductivities of Bare and Bi-coated β''-Al$_2$O$_3$ at each temperature during the cycle 2. e) Arrhenius plot (AC) of the Na$^+$ ion conductivities of Bi-coated β''-Al$_2$O$_3$ at each temperature during 4 cycles.

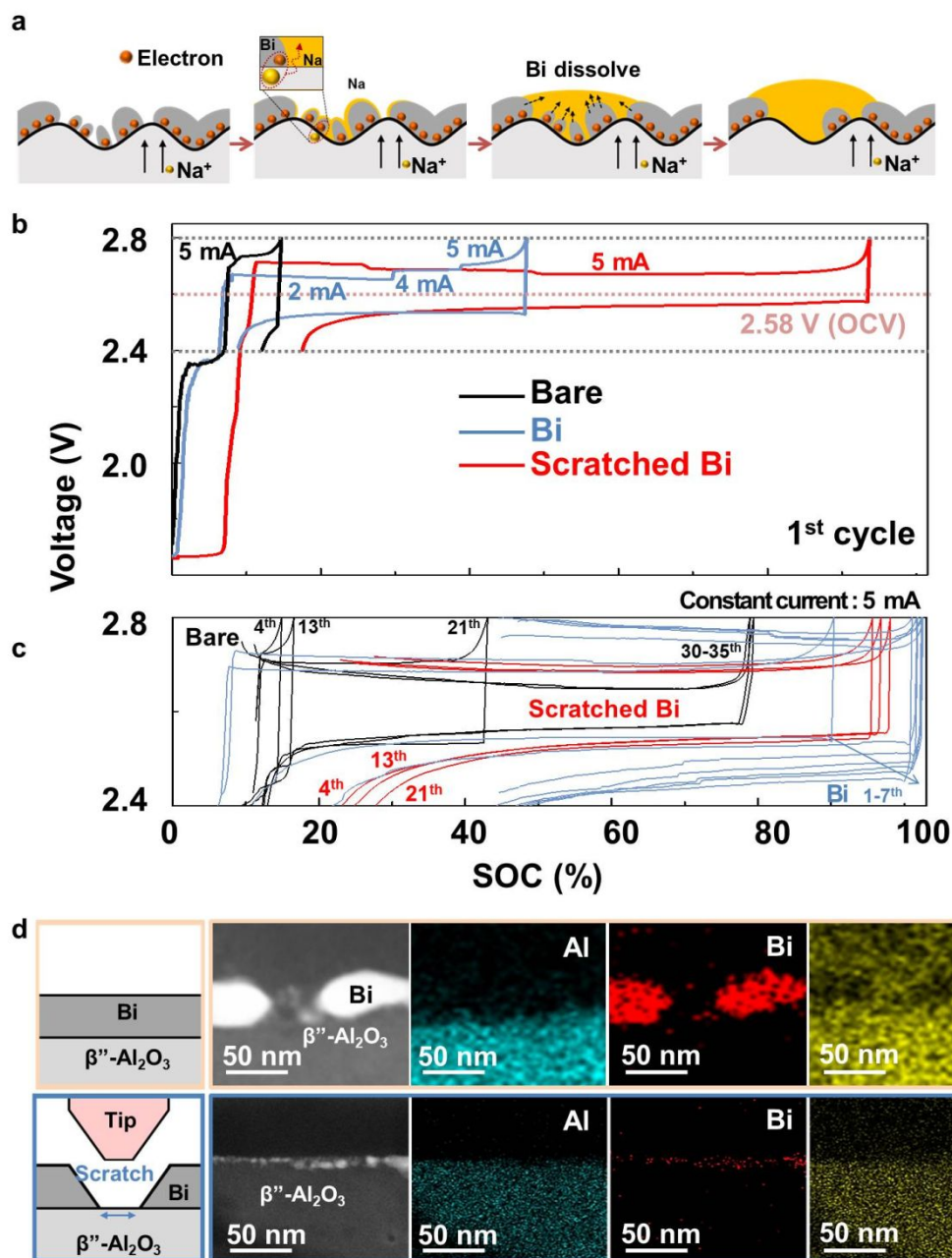**Figure 5.** a) Schematic of the Na-filling process of scratched, Bi-coated β''-Al$_2$O$_3$ cell on charging. b) Voltage profiles of the initial cycle of bare, Bi-coated, and scratched Bi-coated β''-Al$_2$O$_3$ cell. The Bi-coated sample was charged, with an increasing current of 0.6 mA (for 2 h), 1 mA (for 10 h), 2 mA (for 17 h), 4 mA (for 4 h), and 5 mA (until the cell voltage reached 2.8 V). For the bare and scratched Bi-coated cases, 0.6 mA (for 2 h), 1 mA (for 10 h), and 5 mA

(constant) were used. c) Voltage profiles of Bi-coated (for 7 cycles), scratched Bi-coated (for 21

cycles) and bare β''-Al$_2$O$_3$ cell (for 35 cycles). d) Cross-sectional schematic, TEM image, and

high resolution EDS elemental mapping of the scratched Bi-coated β''-Al$_2$O$_3$ surface for Al, Bi,

and O, respectively.

TOC graphic